Transactions of the Korean Nuclear Society Autumn Meeting
Gyeongju, Korea, October 25-26, 2012

Formation of Nano-sized ODS Clusters in Mechanically Alloyed NiAl-(Y,Ti,O) Alloys

Kim Yong Deog [a*], Bae Seong Man [a], Brian D. Wirth [b]
a. *KHNP Central Research Institute, 103-16 Munji-dong, Yuseong-gu, Daejeon, Korea*
b. *Department of Nuclear Engineering, University of California, Berkeley, California*
[*] *Corresponding author: gobear@khnp.co.kr*

1. Introduction

This study focuses on designing and developing advanced oxide dispersion strengthened (ODS) NiAl intermetallics with improved high temperature creep strength by incorporating a high number density (~10^{24} m^{-3}) of very thermally stable Y-Ti-O nano-clusters, akin to those recently observed to improve creep strength and radiation resistance in nano-structured ferritic alloys [1-6]. Advanced ODS NiAl alloys have been produced by mechanical alloying of pre-alloyed Ni-50at%Al with Y_2O_3 and Ti elemental powders. The milled powders were subsequently consolidated by spark plasma sintering, with the objective of producing very high number densities of nano-sized Y-Ti-O precipitates, along with fine grain size. Advanced experimental characterization techniques, combined with micro- hardness strength measurement, were used to investigate the material microstructure and strength following processing. In particular, the size, number density and composition of nano-clusters were assessed.

2. Experimental Methods

This section describes the details of the materials processing that were performed during fabrication of ODS NiAl.

2.1 Mechanical alloying

In this study, ODS NiAl raw matrix materials were prepared from prealloyed, gas-atomized Ni-50at% Al powders supplied by Crucible Industries LLC. Y_2O_3 and Ti particles were added as dispersoid elements. All three powders have the same particle size of -325 mesh and purity of 99.99%. NiAl, Y_2O_3, and Ti powders respectively. Mechanical alloying was performed for these three compositions with 100Cr6 steel ball media under Ar gas sealed environment. The milling speed was set to 1200 rpm (linear speed of 11 m/sec) and the milling times to investigate an optimum powder alloying condition were 2, 5, 10, and 15 hrs respectively.

The high energy milling machine, Simoloyer-CM01 was used. Figure 1 shows a high energy attrition mill, Simoloyer CM-01, and schematic gas and water flow.

2.2 Spark Plasma Sintering (SPS)

The SPS process [7] is a combination of conventional electric-current sintering and hot-pressing based on high temperature plasma instantly generated in the gaps between powders by electrical discharge current. In this study, SPS method was utilized to consolidate the ODS NiAl alloys with improved high temperature strength. Densification behavior, micro-structure and mechanical properties of the consolidated alloy specimens will be discussed in this presentation.

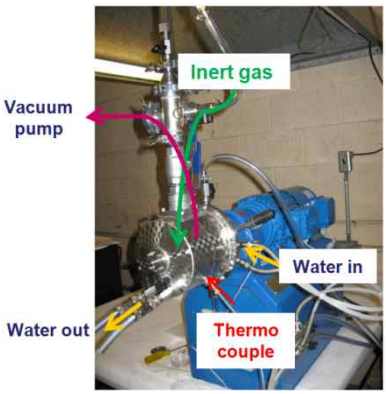

Figure 1. Simoloyer CM-01 high energy attrition mill

3. Characterization Results

Various experimental characterization techniques, scanning electron microscopy, X-ray diffraction (XRD), energy dispersive spectroscopy, transmission electron microscopy, atom probe tomography were used to investigate the material microstructure. As well, Vickers microhardness measurement was used to assess the basic mechanical property of the alloys. The microstructural characterization results of as-milled and as-consolidated NiAl alloys to assess the optimal milling time are discussed in this chapter. Besides, the effort has gone into rationalizing the relationship between the strength and the microstructure of the ODS NiAl alloys.

3.1 X-ray diffractometry

Figure 2 illustrates the evolution of XRD as a function of milling time for three NiAl alloy powder blends. Bragg diffraction peaks of NiAl, Y_2O_3 and Ti are clearly visible for the initial powder mixtures but the peaks of alloying elements, Y_2O_3 and Ti, cannot be revealed for the powders after 2 - 10 hour ball milling. It is considered that more than 2 hour of milling time led to the disappearance of the XRD peak for Y_2O_3 and Ti caused by dissolution into the NiAl matrix. Grain size, strain, and dislocation densities estimated as a

function of milling time will be discussed in the presentation.

3.2 Scanning electron microscopy (SEM)

Figure 3 shows typical SEM micrographs of the NiAl-1wt%Y_2O_3-1wt%Ti composition powders before and after the ball milling using a Hitachi S-4300 SEM machine with 20kV accelerating voltage. Figure 3(a) shows the micrographs of elemental mixture powders before the ball milling. The powders are spherical shape and have various sizes of 5 – 40 μm. After 2 hr ball milling (Figure 3(b)), the powders are uniformly refined and have a flake shape less than 10 μm. After 5 -15 hr ball milling, the powders have sizes of 5 – 10 μm. There is no significant change in size and shape after 5 hr ball milling.

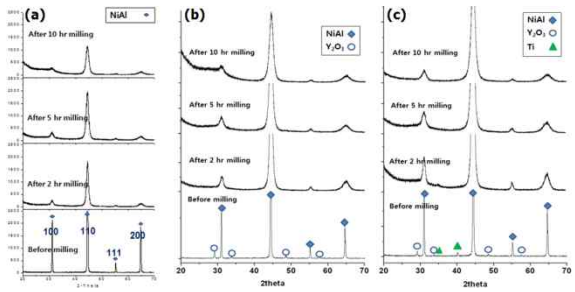

Figure 2. XRD patterns of the mechanically alloyed powders as a function of milling time (a) NiAl (b) NiAl-1wt%Y_2O_3 (c) NiAl-1wt%Y_2O_3-1wt%Ti

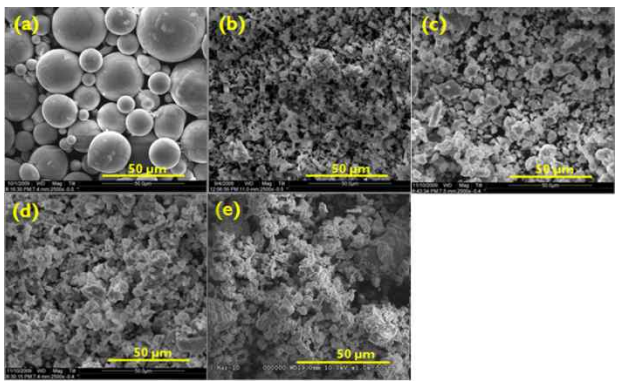

Figure 3. SEM micrographs of NiAl-1wt.%Y_2O_3-1wt.%Ti powder as a function of milling time; (a) before milling (b) 2 hr (c) 5 hr (d) 10 hr (e) 15 hr ball milling

3.3 Consolidated specimen characterization

Vickers microhardness measurement was performed to characterize the basic mechanical properties of the ODS NiAl alloy materials. Figure 4 shows the microhardness results of the SPSed NiAl alloys as a function of the milling time. The results can be summarized as follows: The addition of Y_2O_3 results in smaller increases in microhardness than for additions of both Y_2O_3 and Ti. The microhardness increased with increasing milling time up to 5 hrs and then saturated. The main microstructural contributions to this microhardness, or strength, of these alloys are believed to be grain refinement and particle strengthening. A quantitative relation between the microstructure and microhardness will be discussed in the presentation.

3.4 Transmission electron microscopy (TEM)

TEM analysis of the as-consolidated NiAl alloys after ball milling for 10 hr was conducted to investigate

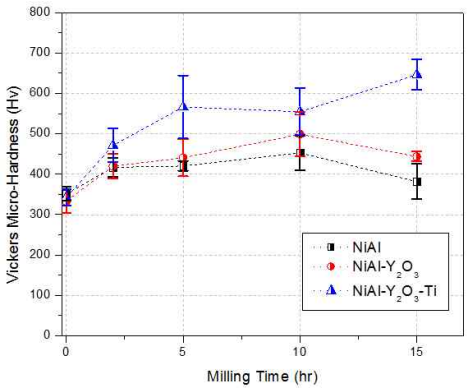

Figure 4. Vickers microhardness test results of the consolidated NiAl specimens as a function of milling time

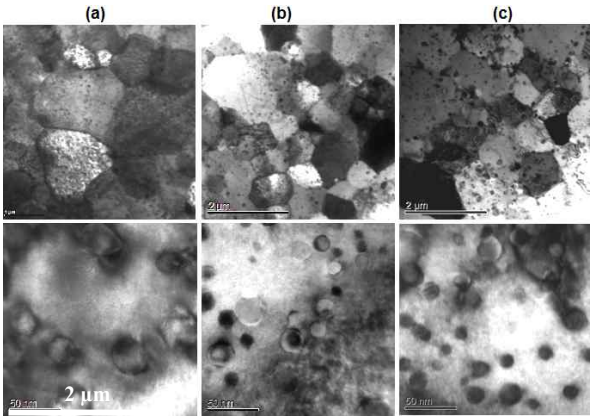

Figure 5. TEM micrographs of the as-consolidated NiAl alloys, (a) NiAl (b) NiAl-1wt%Y_2O_3 (c) NiAl-1wt%Y_2O_3-1wt%Ti

the microstructure of the ODS NiAl alloys. Figure 5(a)-(c) shows the TEM microstructure evolution of the 10 hr milled and SPS consolidated NiAl alloys. The grain size and precipitate number density, measured by TEM, are summarized in Table 1. The grain size has a multimodal distribution with both fine (< 200 nm) and coarser (> 1 μm) grain regions. The average grain size of the NiAl alloys including either Y_2O_3 or both Y_2O_3 and Ti is smaller than that of the pure NiAl alloy. The tempting conclusion is that the grain growth during the consolidation was definitely controlled by the addition of Y_2O_3 and Ti. The NiAl-1wt%Y_2O_3 and NiAl-1wt%Y_2O_3-1wt%Ti alloys have very similar grain size

distribution. Aluminum oxide particles with sizes around 40 nm were observed in the pure NiAl alloy (Figure 5(a)). Precipitates of 10 to 20 nm size were distributed in both the NiAl-1wt%Y_2O_3 and NiAl-1wt%Y_2O_3-1wt%Ti alloys (Figure 5(b) and (c)). The particle number densities of each alloy were $0.3x10^{22}/m^3$, $0.8x10^{22}/m^3$, and $1.4x10^{22}/m^3$ for NiAl, NiAl-1wt%Y_2O_3, and NiAl-1wt%Y_2O_3-Ti respectively. Despite the high levels of strain introduced by the mechanical alloying, this TEM investigation of the consolidated NiAl alloys rarely found dislocations.

Table 1. Summary of the characteristics measured in the NiAl alloys

Alloy	NiAl	NiAl-Y_2O_3	NiAl-Y_2O_3-Ti
Grain size (μm)	1.04±0.19	0.67±0.12	0.68±0.11
Precipitate N (10^{22} m^{-3})	0.3	0.8	1.4
Precipitate size (nm)	30±7.5	15±6.6	14±6.1
Microhardness(kg/mm^2)	450±42	501±54	550±58

3.5 Atom probe tomography

Atom Probe Tomography (APT) was performed in collaboration with Mike Miller at ORNL. Figure 6 shows a 3-dimensional APT map for the as-consolidated NiAl-1wt%Y_2O_3-1wt%Ti alloy. Such atom maps can provide information on the overall solute distribution as well as the size and composition of fine scale precipitates. As shown in Figure 6, the Ni, Al and Fe elements were homogeneously distributed. There was indication of Y-Ti-O clustering along with some heterogeneous distributions of Y, Ti, and O. Additional APT studies are needed. However, limitations of the time available on the ORNL instruments and challenges of specimen preparation for the LEAP instrument precluded more extensive APT study.

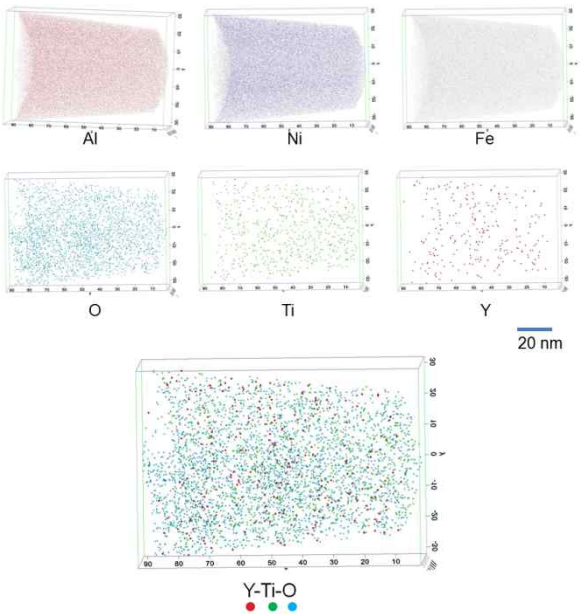

Figure 6. Atom probe tomography images of Al, Ni, Fe, Y, Ti, and O that were observed in the as-consolidated NiAl-1wt%Y_2O_3-1wt%Ti alloy

4. Conclusions

For ODS NiAl alloys, the key observations can be summarized as followings:

1. There was a clear indication that milling for 5-15 hrs was sufficient to produce good mixing during the mechanical alloying process, as determined by XRD, SEM, and EDS results.
2. Powder consolidation was carried out by spark plasma sintering. Fully dense NiAl alloy materials were produced by SPS.
3. A distribution of 10-20 nm precipitates was found in NiAl-Y_2O_3 and NiAl-Y_2O_3-Ti alloys, and those precipitates were identified as Y-Al-O (garnet) particles in the NiAl-Y_2O_3, while both garnet ($Y_2Al_4O_7$) and $Y_2Al_9Ti_2O_6$ phase particles were found at the NiAl-Y_2O_3-Ti alloy.
4. The Al composition of a particle increases as the particle size increases, and Y was dominantly found at the particles size of less than 50 nm while Ti was found at the relatively larger particles with size larger than 100 nm. The Al incorporation believed detrimental to the formation of nanoscale Y-Ti-O precipitates.
5. The effect of Hall-Petch grain size and dispersion strengthening mechanisms in ODS NiAl alloys will be semi-quantatively assessed.

REFERENCES

[1] Ukai, S., et al., *ALLOYING DESIGN OF OXIDE DISPERSION-STRENGTHENED FERRITIC STEEL FOR LONG-LIFE FBRS CORE MATERIALS.* Journal of Nuclear Materials, 1993. 204: p. 65-73.

[2] Alinger, M.J., G.R. Odette, and D.T. Hoelzer, *The development and stability of Y-Ti-O nanoclusters in mechanically alloyed Fe-Cr based ferritic alloys.* Journal of Nuclear Materials, 2004. 329: p. 382-386.

[3] Okuda, T. and M. Fujiwara, *DISPERSION BEHAVIOR OF OXIDE PARTICLES IN MECHANICALLY ALLOYED ODS STEEL.* Journal of Materials Science Letters, 1995. 14(22): p. 1600-1603.

[4] J. Bentley, D.T.H., D.W. Coffey and K.A. Yarborough, *EFTEM and Spectrum Imaging of Mechanically Alloyed Oxide-Dispersion-Strengthened 12YWT and 14YWT Ferritic Steels.* Microscopy and Microanalysis, 2004: p. 662-663

[5] Yamashita, S., et al., *Formation of nanoscale complex oxide particles in mechanically alloyed ferritic steel.* Philosophical Magazine Letters, 2004. 84(8): p. 525-529.

[6] Jiang, Y., J.R. Smith, and G.R. Odette, *Formation of Y-Ti-O nanoclusters in nanostructured ferritic alloys: A first-principles study.* Physical Review B, 2009. 79(6).

[7] TOKITA, M., *Mechanism of spark plama sintering.* Proceedings of 2000 Powder Metallurgy World Congress, 2000.